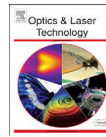




Contents lists available at SciVerse ScienceDirect

Optics & Laser Technology

journal homepage: www.elsevier.com/locate/optlastec

Review

A review of visible-range Fabry–Perot microspectrometers in silicon for the industry

João Paulo Carmo^{a,*}, Rui Pedro Rocha^a, Marian Bartek^b, Ger de Graaf^b, Reinoud F. Wolffenbuttel^b, José Hígino Correia^a^a University of Minho, Department of Industrial Electronics, 4800-058 Guimarães, Portugal^b Delft University of Technology, Faculty of EEMCS, Department ME/El, Mekelweg 4, 2628CD Delft, The Netherlands

ARTICLE INFO

Article history:

Received 30 December 2011

Received in revised form

23 March 2012

Accepted 26 March 2012

Available online 12 April 2012

Keywords:

Microspectrometer
Integrated silicon microsystem
Industrial applications

ABSTRACT

This review presents microspectrometers in silicon for the industry for measuring light in the visible range, using the Fabry–Perot interferometric technique. The microspectrometers are devices able to do the analysis of the individual spectral components in a given signal and are extensively used on spectroscopy. The analysis of the interaction between the matter and the radiated energy can found huge applications in the industrial sector. The microspectrometers can be divided on three types, determined by the dispersion element or the used approach and can be found microspectrometers based on prisms, gratings interferometers. Both types of microspectrometers can be used to analyze the spectral content ranging from the ultraviolet (UV, below 390 nm), passing into the visible region of the electromagnetic spectrum (VIS, 390–760 nm) up to the infrared (IR, above 760 nm). The microspectrometers in silicon are versatile microinstruments because silicon-compatible techniques can be used to assembly both the optical components with the readout and control electronics, thus resulting high-volume with high-reproducibility and low-cost batch fabrications. A compensation technique for minimizing the scattered light effects on interferometers was implemented and is also a contribution of this paper. Fabry–Perot microspectrometers for the visible range are discussed in depth for use in industrial applications.

© 2012 Elsevier Ltd. All rights reserved.

Contents

1. Introduction	2312
2. Microspectrometer's taxonomy	2313
3. Grating microspectrometers	2314
4. Interferometric microspectrometers	2314
4.1. Microspectrometer design	2314
4.2. Case study	2315
4.3. Limitations	2317
4.4. Compensation of scattering non-idealities	2318
5. Conclusions	2319
References	2319

1. Introduction

The developments in the microelectronic field observed on last years resulted in an increased well being for the mankind. This is

especially true when looking for almost all aspects of the human life, where it is possible to find microelectronic devices and microstructures whose fabrication were impossible without the currently available fabrication techniques [1–7]. In this context, new industrial applications of Microsystems made possible the development and proliferation of low-power wireless devices with reduced dimensions for data and sensory communications [8], object tagging and components for chain fabrication facilities [9],

silicon-compatible microbatteries [10] for micropowering and photonic applications [11–13]. However and despite the huge and fascinating range of applications for microsystems, the most challenging is undeniably those one used to detect and/or manipulate the light. This idea backs to the second century before our age, when Archimedes planned to destroy enemy ships using a solar heat ray with an array of actuators to change the shape of a mirror [14]. The field of photonics is one that offers the possibility to achieve one of the greatest realizations and applications because the light is present in all aspects of the human life and our way of living is impossible without light. A detailed search for microsystems application in the industry allows concluding that the spectroscopy is the field where the use of optical sensors is essential.

Spectroscopy is the science of studying the interaction of light with matter as a function of the wavelength, λ [nm]. The state of electrons in atoms and molecules can be changed due to the interaction between the light and the matter. In this case, the exchanging of energy between them can result in one of the following effects: scattering, emission or absorption of light [15]. The spectrography is a well-established technique in several fields of science (e.g., physics, chemistry and biology) and can be applied in virtually almost applications. The near infrared (NIR) spectroscopy analyses the spectral region located between 700 nm and 2500 nm [16] and can be used for monitoring the quality control of food and beverages [17], as well as for detecting counterfeit medicines [18]. The spectral region located between 1.4 μ m and 10 μ m is the so-called mid infrared (MIR) range and it can be used in the agriculture for quantitative analysis of soil contents [19] as well as for doing quality control in the food industry by detecting oils and/or fats [20]. The MIR spectroscopy can also be used with success by criminalist investigators for doing forensic analysis of several kinds [21]. It is possible applying spectroscopy methods in the visible range of the electromagnetic spectrum. The visible range is a small part of the entire electromagnetic spectrum located between 390 nm and 760 nm and the only part which can be perceived by the human eye. Many applications require spectral analysis at the visible wavelengths: inspection of product defects in the industry by means of color determination, biochemical analysis (e.g., physiological fluid, human blood, muscle tissue, DNA fibers) [22], light scattering by materials (liquids, plastics, polymers and gels), and so on. It is also possible to use the energy-dispersive X-ray spectroscopy (EDS or EDX) technique for doing the characterization of environmental particles [23], but its usage is out-of-the-scope of this paper. A microspectrometer is an instrument that separates the light into its basic spectral components [24] for analysis.

It is commercially available few high-performance multiple-grating spectrometers featuring impressive spectral resolutions, $R = \lambda/\Delta\lambda$, that easily exceeds $R = 10^6$, where $\Delta\lambda$ [nm] is the -3 dB power bandwidth (also known as the full-width half-maximum, FWHM) for a particular settled wavelength, λ [nm], but only very specific applications such as those required by the astronomy require such spectral resolutions [25]. Furthermore, the strong dependence of the quantity R with the resolving power capability makes it the most important indicator of a spectrometer. The spectral resolutions found in microsystems based on assembled MEMS and based on integrated silicon components are typically limited by $R = 100$ and $R = 20$, respectively [26]. Fortunately, the majority of the industrial applications (including the formerly cited) require smaller spectral resolutions that do not exceed few dozens. The main consequence of this is the huge industrial potential of microspectrometers, where its small size and cost more than compensates their R -limitation [27].

This review presents visible-ranged microspectrometers based in the Fabry–Perot interferometric technique for the industry, and is followed by a discussion on the limitations imposed to these

devices. An array-type microspectrometer for the visible is present as a case study. A compensation technique to minimize the effect of the scattered light was implemented and is also a major topic of discussion.

2. Microspectrometer's taxonomy

Since spectrometers work with the optical domain, specific techniques are required for processing the wavelength components of the light beam. A wavelength separator of some kind can be found in a spectrometer and depends from the used dispersion element. This leads to three know types of spectrometers: these one based on prisms, on gratings and on interferometers. The first type requires long optical paths and thus, it is not suitable for fabricating microspectrometers.

Fig. 1 shows simplified schematics of typical grating and interferometric type microspectrometers. In a grating type microspectrometer, the incident passes by an entrance slit and is dispersed by way of a grating [15]. Normally, the diffraction gratings are composed of closely spaced transmitting slits on a

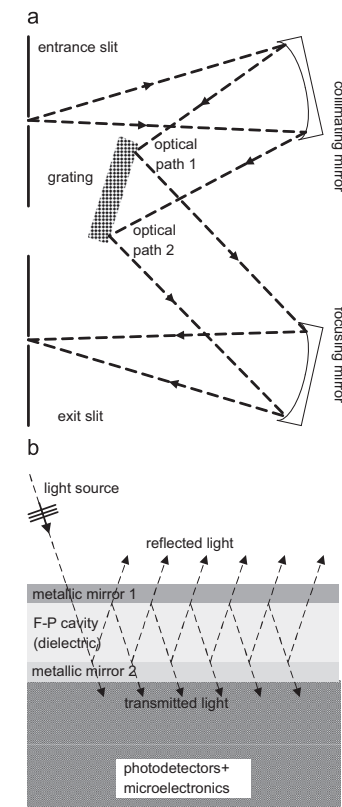


Fig. 1. Simplified schematics illustrating the principle of (a) grating and (b) interferometric (a Fabry–Perot cavity) microspectrometers.

* Corresponding author. Tel.: +351 253 510190; fax: +351 253 510189.
E-mail address: jcarmo@dei.uminho.pt (J.P. Carmo).

flat surface (also known as transmission gratings) [28] or alternate reflecting and non-reflecting grooves on a flat or curved surface (the reflection gratings) [29]. For the case of microspectrometer based on interferometers, the dispersion of the incident light is done by splitting it on several components and putting them traveling several optical paths. After their recombination, these components interfere constructively only if their path difference is an integer quantity of a selected wavelength. This means that an interferometer is a device that acts as a filter for transmitting certain wavelengths and reflecting (rejecting) the others back to the light source. It exist at least four types of interferometric techniques (e.g., Michelson [30], Mach-Zender [31], Sagnac [32] and Fabry–Perot [33]). The most promising approach for fabricating interferometer type microspectrometers is using Fabry–Perot interferometer (also known as Fabry–Perot etalon) for acting as a dispersion element - see Fig. 1(a). This is true because the interferometer can be mounted on top of microelectronic devices (CMOS and/or bipolar) using IC-compatible fabrication techniques (deposition techniques of both dielectric and metal layers, etching techniques (e.g., bulk micromachining using wet solutions of potassium hydroxide solutions — KOH — and dry micromachining by way of reactive ion etching — RIE) [26].

3. Grating microspectrometers

Grating microspectrometers are generally fabricated using bulk micromachining techniques (either with KOH alkaline solutions or RIE techniques). The roughness resulted on micromachined surfaces make these type of microspectrometers to be very difficult to fabricate and to reproduce their spectral characteristics. Moreover, high-quality gratings are required to match the targeted resolutions and can take two types of shapes: transmission slits [34] and reflective gratings [35] arrays. The need of dedicated processing steps for obtaining diffraction gratings is the main limitation associated to the fabrication of these microspectrometers. It must be noted that these kind of microspectrometers are more suitable for separating the light in the infrared (IR) range and behind (i.e., outside the visible range). In this sequence of ideas, the microspectrometers based on interferometric techniques constitute cheaper and simpler approaches.

4. Interferometric microspectrometers

4.1. Microspectrometer design

Fabry–Perot etalons (FPEs) are structures widely used for separating a specific wavelength from a broad band light source. FPEs are composed by two highly reflective surfaces (e.g., two parallel mirrors) facing each other and a dielectric resonant cavity in-between those with a selected distance d [m]. There are two methods to fabricate such structures. One method is stacking a given number of dielectric layers, which defines the properties of the mirror but having a very complex and hard to control fabrication process due to the number of layers (and their thicknesses) required for defining the full width half maximum (FWHM). The other method uses two plasmonic waveguides in the following interfaces: air/resonance cavity and resonance cavity/photodetector. Because the thickness of the metallic mirrors is in the nanometer range, the light transmission between dielectric mediums is done through the mirrors working as plasmonic waveguides [36]. Simultaneously, these mirrors work as highly reflecting surfaces inside the cavity (e.g., the light resonate due to successive reflections) [37]. The optimum result obtainable when working with FPEs is dependent on the light

source beam and the generic homogeneity and smoothness of the fabricated structure. This type of devices is fabricated by stack-like thin-film deposition techniques inducing even more stray-light in the FPE environment due to the interface surfaces' roughness caused by the fabrication processes. The contact interfaces between layers are critical in quantifying the light scattering phenomenon that decreases the efficiency in the spectral selectivity expected for these resonant cavities.

The spectral selectivity of a FPEs depends directly on the finesse, F_{int} , of the resonator. It is desirable to have the highest possible value of F_{int} in order to increase the resolution. The finesse of parallel mirrors is given by:

$$F_{int} = \pi r^{1/2} \times (1-r)^{-1} \quad (1)$$

where r is the reflection coefficient of the mirrors. The most relevant aspects when designing such devices are the ability to fabricate flat mirrors with high reflectivity and at the same time guaranteeing that the two are parallel to each other. The resolution depends on the incidence angle of the light entering the cavity (for a given wavelength) and takes the maximum value when the parallelism of mirrors is perfect. This enhances the number of reflections and at the same time, this increases the number of interferences with the consequent finesse improvement. The spectral information can be obtained simply by varying the variables intrinsically associated with the resonator, whose values are (under ideal conditions) given by:

$$q\lambda = 2nd\cos(\alpha) \quad (2)$$

where q is an integer number that gives the interference order, α [°] or [rad] is the angle of incidence, n is the refractive index inside the cavity and d [m] is the distance between the mirrors. The resonance in the cavity occurs at $2nd = q\lambda_0$. It should be noted that such devices are designed for $q=1$ for application in the visible spectrum. As illustrated in Fig. 2, the distance between the mirrors must be within the 200–390 nm range, for operation in the visible spectrum with $q=1$. The distance between mirrors (for the same wavelength range) decreases when the dielectric material that forms the cavity is replaced by another one with a higher refractive index. This means that using silicon dioxide, the distance between the mirrors must decrease in accordance for

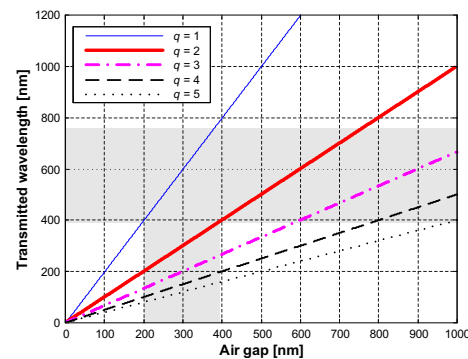


Fig. 2. Transmitted wavelength versus air gap ($n=1$) between mirrors. The visible range is in the horizontal shading. The cavity width must be in the range 200–390 nm ($q=1$) for allowing only one wavelength (vertical shading) in the range 400–780 nm to pass through it.

still covering the visible spectrum. This happens because the refractive index of this material ($n=1.46$) is higher than of the air ($n=1$).

The FPEs design was done in a way to allow their integration with the electronics of control and optoelectronic conversion. In this context, the aluminum (Al) was the selected material for the bottom mirror due to its compatibility with microelectronics processes (either CMOS or bipolar) [36,38]. The aluminum could be also a suitable candidate for the top mirror, but unfortunately this material presents higher absorption losses in the visible when compared with silver (Ag) [36,38]. Contrary to what happens in the macroscopic scale, a good protection from environmental exposition must be provided (for example, by sealing the complete microsystem) for avoiding any type of mirror degradation. In this sequence of ideas, it must be noted that to perform the spectral analysis, both the aluminum and silver mirrors cannot be opaque in order to allow the light to enter into the resonating cavity. This semi-transparency state is what will allow the light to enter into the etalon and resonate inside the cavity and reflect back and forth as many times as possible until exiting. The number of reflections and transmissions occurring during the resonating time evaluates the effect of the wavelength's interference until it is completely dissipated. The silicon dioxide (SiO_2) is transparent enough to allow the light to resonate within dielectric cavities and at the same time it is simple to deposit above the bottom mirror. This makes the silicon dioxide a suitable material for fabricating the dielectric cavities. Moreover, the silicon dioxide presents a constant refractive index approximately of 1.46 in the visible region, which is an added advantage for applications working in this particular portion of the electromagnetic spectrum. Since different wavelengths have different penetration depths, it means that shorter wavelengths will have smaller penetration depths. Fig. 3(a) shows this concept. This simplifies the fabrication of matrices of cavities (each single cavity for a single photodetector) with different thicknesses of silicon dioxide [39]. The summary of the main characteristics (optical, electronic and mechanical) of this microspectrometer can be found in Table 1.

Alternatively and as illustrated in Fig. 3(b), a tapered cavity (above a large number of photodetectors) with a continuously variation in the thickness profile also constitutes an interesting idea for fabricating microspectrometers [40]. Independently of the used fabrication processes, the cavities must resonate within the visible spectrum. The Fabry–Perot interferometer fabricated by Emadi et al. [40] was designed to cover the spectrum between 570 nm and 720 nm. These specifications were achieved by fabricating cavities with its thickness varying linearly between 850 nm and 1000 nm. For this reason, this interferometer was denominated as Linear-Variable Optical Filter (LVOF). Moreover and contrary to what is usual, the mirrors were fabricated using layers made of different dielectric materials with different thicknesses. Each mirror contains five alternate layers of titanium dioxide (TiO_2) and silicon dioxide (e.g., three layers of TiO_2 and two layers of SiO_2 with 67 nm and 112 nm, respectively). The LVOF was tested with the help of a commercial CCD digital camera, by attaching it into the camera's objective and selecting the wavelength of a light source. A monochromator was used for this purpose. Then, a successive number of snapshots were acquired for further analysis, as well as for calibrating the whole system (composed by the LVOF and the camera). This is not a true-silicon microspectrometer. However, this opens good perspectives for future fabrication of complete microspectrometers because the techniques and the materials used for fabricating the LVOFs are compatible with those used by the microelectronics industry (either CMOS or bipolar or both). Table 1 also lists the main characteristics of this approach.

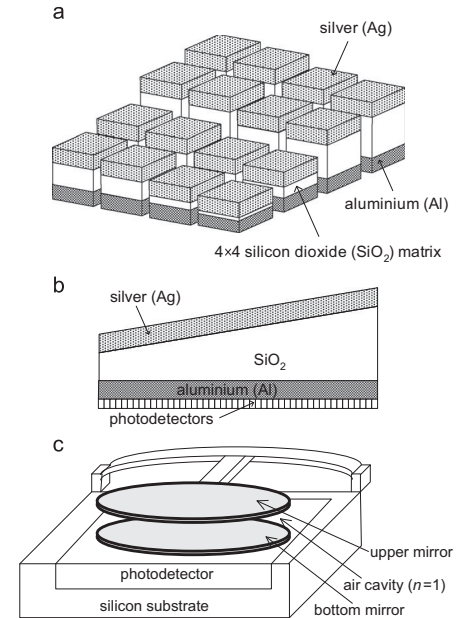


Fig. 3. Approaches for obtaining Fabry–Perot integrated microspectrometers used by (a) Correia et al. [39], (b) Emadi et al. [40], and (c) Chang et al. [41] (for convenience of illustration, only one Fabry–Perot etalon with air cavity is showed).

A previous attempt using the air ($n=1$) as the material within the cavities array was achieved by Chang et al. [41]. This microspectrometer contains 16 photodetectors (forming a 4×4 matrix of photodetectors) made of lateral interdigit PIN diodes, which were fabricated on a High Resistive Silicon (HRS) substrate for providing high isolation between adjacent photodetectors. As illustrated in the artwork of Fig. 3(c), the mirrors are both made of silver with a thickness of 50 nm and presenting a circular shape. The main difference between the mirrors relies in the selected materials for providing mechanical adaptation. The bottom mirrors are supported on a $1 \mu\text{m}$ -thick silicon nitride (SiN) layer, whereas each of the top mirrors are suspended by a 50 nm-thick silicon dioxide pre-buckled bridge. The width of the air cavities are in the range 140 nm and 290 nm for detecting light within the 400–680 nm range. The summary with the main characteristics of this microspectrometer can also be found in Table 1.

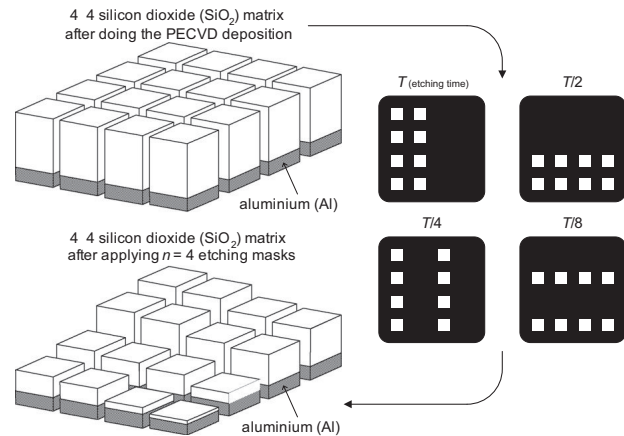
4.2. Case study

Fig. 4 illustrates the array with 16 resonators (i.e., the 4×4 Fabry–Perot etalons array) without the upper mirror [39]. This Figure clearly illustrates this concept, whose result is the thinning of silicon dioxide layers into 16 channels with different thicknesses. The white squares in black masks are holes that were drilled in order to allow the plasma etching of the silicon dioxide. The Scanning Electron Microscope (SEM) photograph in Fig. 5(a) shows a cross section of one of the fabricated Fabry–Perot etalons, where it is possible to observe the resonant cavity made of silicon dioxide layer between the top silver

Table 1

Summary of the several approaches for obtaining Fabry–Perot microspectrometers.

	Correia et al. [40]	Emadi et al. [39]	Chang et al. [41]
Chip-area	3.9 × 4.2 mm ²		
FWHM	18 nm	0.2 nm	
Technology	1.6 μm CMOS	LVOF mounted on a CCD Canon EOS 10D digital camera	Lateral interdigit PIN diodes
Wavelength range (nm)	380–500	570–720	400–680
Photodetectors (PDs)	P ⁺ /N-well photodiodes	Individual CCD pixels of the digital camera	Lateral interdigit PIN diodes on a HRS substrate
Number of PDs	16: 4 × 4 matrix	13: 200 pixels within 13 groups of 15 pixels	16: 4 × 4 matrix
Dark current (fA)	30		633
Size of PDs	500 × 500 μm	75 μm: groups of 15 pixels in a 5 μm pitch	< 160 μm
Mirror types	Metallic materials	Dielectric materials	Dielectric metallic mixed materials
Top mirror materials	Silver (Ag)	Alternate layers made of titanium dioxide (TiO ₂) & silicon dioxide (SiO ₂)	Silicon dioxide (SiO ₂) bridge/silver (Ag)
Bottom mirror materials	Aluminum (Al)	Alternate layers made of titanium dioxide (TiO ₂) & silicon dioxide (SiO ₂)	Silicon nitride (SiN)/silver (Ag)
Thickness of Top/Bottom mirrors (nm)	45 nm/20 nm	TiO ₂ /SiO ₂ /TiO ₂ /SiO ₂ /TiO ₂ 67/112/67/112/67 nm total thickness = 425 nm	50 nm of SiO ₂ and 50 nm of Ag/1 μm of SiN and 50 nm of Ag
Cavity materials	Silicon dioxide (SiO ₂)	Silicon dioxide (SiO ₂)	Air
Refractive index, <i>n</i> , of cavities	≈ 1.46	≈ 1.46	≈ 1
Thickness range of cavities (nm)	225–300, step=5 nm	850–1000, linear thickness variation	140–290

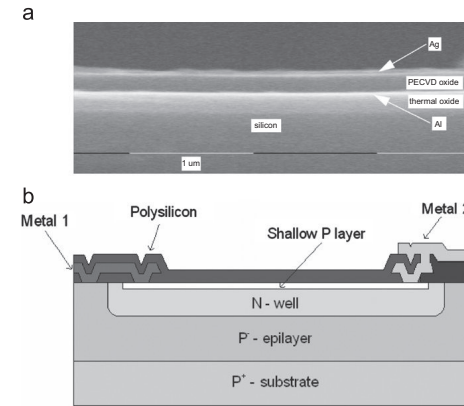
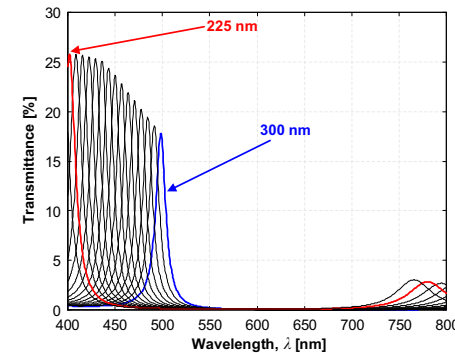
**Fig. 4.** The principle used to form the etalons matrix. After the deposition of the 4 × 4 silicon dioxide matrix, different etching times are used for each mask. The result is a 4 × 4 silicon dioxide matrix with different thicknesses.

and the bottom aluminum mirrors. The artwork depicted in Fig. 5(b) makes clear how the FPEs were deposited on top of the photodetectors (which were fabricated in a 1.6 μm standard CMOS process).

A thin-film optics software package was used for structural optimization of the 16 FPEs because the thickness of the silver layer is a trade-off between the absorption loss and the full-width half-maximum (FWHM). Contrary to what happens under ideal conditions, the simulations already taken in account the effects introduced by the materials used in the mirrors. In this context, the simulations showed that the most suitable thicknesses of mirrors were, respectively, 45 nm and 20 nm for the silver and aluminum. In terms of technology there are no constraints associated to the silicon dioxide, because this material acts as an adaptation layer, ensuring the further coexistence of silver

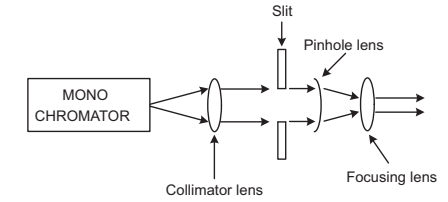
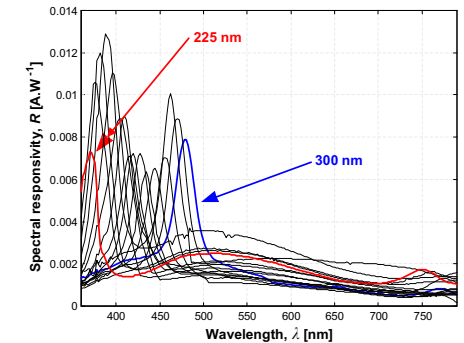
with the microelectronics (e.g., the array of 16 photodiodes). As showed in Fig. 5, the thickness of the 16 dielectric cavities was selected to change from 225 nm up to 300 nm and increasing in increments of 5 nm. This makes possible to cover the 400–500 nm wavelength range with an inter-channel shift of about 6 nm.

The performance evaluation of the device was done by measuring the electrical characteristics and the optical response of each individual channel. The measurement setup was mounted as follows: a light beam sourced by a monochromator (model Triax-180 featuring a 1.2 kg mm⁻¹ grating with a spectral dispersion of 3.6 nm mm⁻¹ for achieving a spectral resolution of 0.3 nm at the 546 nm wavelength) was collimated with the help of a lens. Then a slit, a pinhole and focusing lenses allowed the production of an optical beam with a 400 μm of diameter for testing the 16 channels in the matrix. Both the electrical and

**Fig. 5.** (a) Cross section SEM photograph of a selected sample of Fabry–Perot cavity, which is composed of a SiO₂ layer (with a thickness of 300 nm) between a top silver and a bottom aluminum mirrors. The roughness of the contacting surfaces between the different layers is clearly visible in the device. (b) Artwork illustrating the cross section of the photodetector design in a 1.6 μm standard CMOS process.**Fig. 6.** Simulated transmittance versus the wavelength for a set of 16 Fabry–Perot etalons with mirrors made of silver and aluminum with thicknesses of 45 nm and 20 nm, respectively. The thickness of their dielectric layers made of silicon dioxide is in the 225–300 nm wavelength range and varies in integer steps of 5 nm.

optical characteristics of the 16 channels were measured with the help of a DC source/monitor HP model 4142B (featuring a full-scale ranging from 1 fA up to 1 A with a resolution of 0.1 pA). A commercial photodiode (Hamamatsu model S1336-5BQ) was used for calibrating the measurement system in order to make the measurements the most reliable as possible. To finish, all the measurement hardware was mounted and aligned on top of an optical table with an anti-vibrating system to guarantee the precise focusing of the individual channels. Fig. 7 illustrates the setup for a better understanding.

Fig. 8 shows the spectral responsivity, R [A W⁻¹], of the 16 channels, which were measured for the 400–800 nm wavelength range with the help of the respective on-chip photodiodes. It can be observed that the ratio between the base line and the

**Fig. 7.** Focusing light setup for performance evaluation of the device.**Fig. 8.** Measured spectral responsivity of the 16 channels versus the wavelength.

peak maximum ranges from 4 to 7. It can be also observed that the relatively high scattered light, the beam divergence and the roughness surface are the main causes that affected the background signal. As presented in one of the next subsections, a method to compensate the scattered light will help to reduce the effect of the non-idealities of both the incident light beam and the FPEs. The photography of this array-type microspectrometer for the visible range of the electromagnetic spectrum is showed in Fig. 9.

4.3. Limitations

The spectral range can be extended up to about 571 nm (e.g., to more than 480 nm) by using two adjacent dies with 16 channels each (each die with a 4 × 4 matrix) and doing an initial PECVD silicon dioxide deposition with a thickness of 350 nm. Then, an additional fifth etching mask can be applied in the second die for doing a fifth etching step during a time of $T/16$ s. This simple technique is used to form a 32 channels microspectrometer with a higher wavelength range. This technique can be further extended to yield a device with 64 channels ($T/32$) or even with 128 channels ($T/64$).

The major and obvious limitation of array-type microspectrometers is the high waste of the impinging optical power. This happens because the light is projected into the direction of the microspectrometer and then, it is distributed over the array before the dispersion take place. This means that the optical power delivered to each etalon is inversely proportional to the number of channels. The resolution of the fabricated microspectrometer presented in this paper is thus intrinsically limited to $R=16$. This limited performance is due to only the first-mode ($q=1$) be the one allowed for operation in these type of microspectrometers

with the consequence to have a FWHM equal to the finesse, F_{int} , of the FPE (that is limited by the mirror reflectivity) — see Eq. (2). The thickness of thin-films used for fabricating the mirrors limits the designer's action because IC-compatible materials (as it is the case of the aluminum) must be used at least in the bottom mirrors. The fabrication of good aluminum mirrors is a complex and challenging task because high resolutions require mirrors with high reflectances and at the same time, high throughputs are only achieved with low absorptions. This is evident when looking for the thickness increase of aluminum mirrors from 5 nm to 10 nm, whose consequence is an optical transmission reduction from 90% to only 5% and inversely the reflectivity varies from 10% to 85% [42]. These contradictory factors trade between them and difficult the task to get good mirrors in aluminum, especially when the absorption increases rapidly with the thickness of the metallic layer. Therefore, the consequence is achieving a poor signal-to-noise ratio. Practical devices with FPEs made with metallic mirrors typically present throughput peaks at resonance of only 10%. High-performance (high-reflection/low-absorption) mirrors can be fabricated by combining a multiplicity of layers made of dielectric materials [40]. These dielectric mirrors can be easily assembled on top of microelectronic devices (in CMOS or

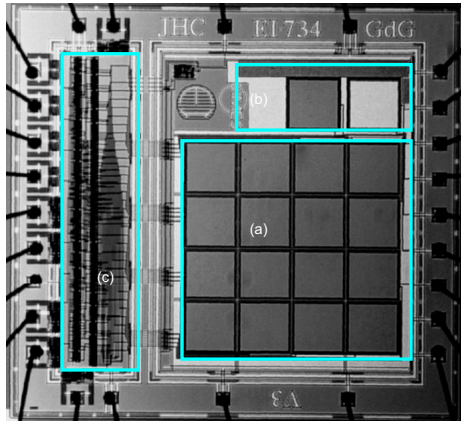


Fig. 9. Photograph of a prototype of an array-type microspectrometer composed by 16 channels, each one with a CMOS photodiode with a Fabry-Perot etalon mounted on top. Three main subsystem blocks can be identified in the photograph: (a) array of 16 Fabry-Perot mounted above 16 photodiodes, (b) dark current reduction, and (c) electronics for readout and signal processing (analog-to-digital conversion and amplification) and a serial bus for communicating with external devices [39].

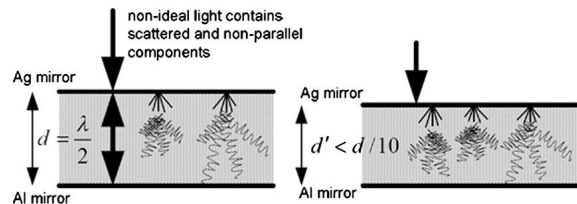


Fig. 10. The optical noise inside a Fabry-Perot etalon, where d [m] is the thickness for resonance to occur for a given wavelength λ [m], and d' [m] is at least ten times thinner than d .

bipolar technology) using IC-compatible thin-film deposition techniques (chemical vapor deposition, CVD) as well as IC-compatible materials (silicon dioxide, SiO_2 , and titanium dioxide, TiO_2) for the several layers of the mirrors [40,43].

Other problems in microspectrometers are the structural induced and the light source noises. The first one happens due to the non-perfectly matching connecting surfaces resulted from the thin-film deposition process where different materials inherently present non-parallelism and roughness. The light source noise problem happens due to the light scattering caused by the non-idealities of Fabry-Perot etalons. A method for compensating this non-ideality will be discussed in detail on the next subsection.

4.4. Compensation of scattering non-idealities

The optimum result obtainable when working FPEs is dependent on the light source beam and the generic homogeneity and smoothness of the fabricated structure. This type of device is fabricated by stack-like thin-film deposition techniques inducing even more stray-light in the FPE environment due to the interface surfaces' roughness caused by the fabrication processes. The contact interfaces between layers are critical in quantifying the light scattering phenomenon that decreases the efficiency in the spectral selectivity expected for these resonant cavities. The non-idealities of this kind of FPEs are responsible for the inherent noise this device presents. This noise is independent from the etalon's thickness and it was noticed that several fabricated devices with different widths present similar noise. Therefore, an improvement of the device's spectral selectivity is obtained by doing the following procedure: first, it is necessary to add an identical passive structure but fabricated to transmit through the etalon a wavelength ten times thinner than the one filtered by the active FPE.

Due to the thin-film deposition process, the non-perfectly matching interfaces of different materials inherently present non-parallelism and surface roughness, detailed in Fig. 6(a). These plasmonic waveguides are the critical part of the FPE to be improved because they better represent the non-idealities of the fabricated device. Nevertheless, it is possible to reduce the overall roughness of the silver surface by applying a pretreatment with a SnCl_2 solution and low iodination temperature [44]. This is very important to do in the silver plasmonic waveguide because it is where the light enters the etalon and the scattering starts immediately after the first contact of the light with the optical cavity. In Fig. 10 is demonstrated how the light interacts inside the cavities with different thicknesses, and the corresponding optical output, caused mainly by two reasons. One is related to the way light travels through different mediums. As light crosses the different layers that compose the FPE, the aforementioned issues induce diffuse reflection. For the visible range, when the free-space incident light reaches the SiO_2 filtering cavity, it will shorten the wavelengths by the medium's refractive index. The other source for noise in the optical filter is caused by the

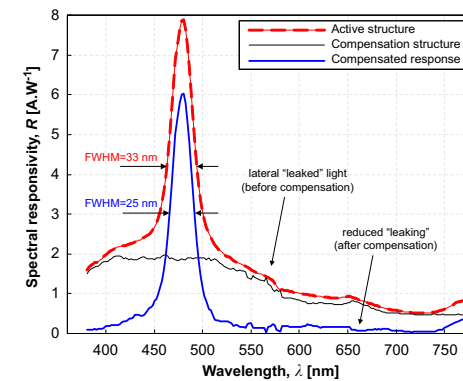


Fig. 11. Mean values of measured spectral responsivities (dashed line) for 300 nm thick FPEs and noise (thinner line) for 30 nm thick compensation FPEs. The "clean" compensated output signal after noise subtraction is also presented (thickest line). It can be observed that the mean FWHM centered at 480 nm was improved by 8 nm (e.g., from 33 nm to 25 nm).

light source's components that are not perpendicular to the filter's plane, which ideally should be. The non-normal components of the light, with unknown angles of incidence, induce multiple reflections inside the cavity [45]. In controlled environments, a collimator is used to minimize the stray light by narrowing the beam, therefore, the presented compensation cavity overcomes these limitations. For the visible wavelengths, the different roughness for each layer are responsible for scattering the light noticeably, visible wavelengths, the different roughness for each layer are responsible for scattering the light noticeably, hence prejudicing the FPE's ability to distinguish a narrow tuned wavelength.

The proposed solution is a ten fold reduction in the thickness of the resonant cavity. Apart from that, this structure is exactly the same as the active FPE. The Ag/SiO_2 interface presents roughness caused by the fabrication processes, which is responsible for the light scattered into plasmonic modes in that region and, ultimately, also for the 8 nm FWHM width improvement. By using such a compensation structure with the only purpose of quantifying the noise and subtract it from the measured signal of the FPE, a reduction of the transmitted spectral band around the resonance wavelength is achieved. This is possible because the fabricated FPEs have similar background noise. Fig. 11 shows the mean values of spectral responsivities [mA/W] measured for all active FPEs and the noise compensation FPEs with thicknesses with 300 nm and 30 nm, respectively. The improved output signal obtained after the subtraction is also represented in Fig. 11. Moreover, Fig. 11 also shows that the FWHM, before and after compensation, is improved by 8 nm hence increasing considerably the device's spectral selectivity. Furthermore, when operating in the visible part of the spectrum, the new passive FPE does not present any new resonance peaks at shorter wavelengths. Therefore, there are not undesirable consequences in adopting such a structure to measure the non-resonant effects and use them for signal compensation purposes.

5. Conclusions

This paper made a review of microspectrometers in silicon for the industry. The technical issues and challenges concerning their

fabrication were also presented, as well as the limitations imposed by their intrinsic dimensions. A compensation technique for minimizing the effect of the scattered light was also presented in this paper. By fabricating a compensating structure producing a background noise similar to the active FPE, the otherwise unwanted signal is then subtracted resulting in a better output signal than without the compensation FPE. The compensation etalon also results in a considerable improvement in the device's spectral selectivity by reducing the FWHM from 33 nm to 25 nm. This solution was applied to a set of FPEs for a wavelength inside the visible range (e.g., $\lambda_0 = 480$ nm) and resulted in a FWHM improvement in the order of 24%. Adding more etalons will cover the entire 380–780 nm wavelengths. The array-type microspectrometer that was presented as case study can be used with success in the industry for doing. To finish, it must be noted that microspectrometers in silicon offer the opportunity to integrate the spectrometer, the readout and signal processing subsystems in the same die in order to provide a genuine microdevice with low-cost.

References

- [1] Jia S, Ding G, Zhao X, Yang C. Novel optic-fiber switches based on the wobble-type MEMS electromagnetic microactuator. *Optics & Laser Technology* 2007;39(2):353–8.
- [2] Li Y, Chen D, Yang C. Sub-microns period grating couplers fabricated by silicon mold. *Optics & Laser Technology* November 2001;33(8):623–6.
- [3] Feng L, Sihal C, Huan L, Yifan Z, Jianjun L, Yiqing G. Fabrication and characterization of polydimethylsiloxane concave microlens array. *Optics & Laser Technology* 2012;44(4):1054–9.
- [4] Shalaby MM, Abdelmonem MA, Saitou K. Design of spring coupling for high-Q high-Frequency MEMS filters for wireless applications. *IEEE Transactions on Industrial Electronics* 2009;56(4):1022–30.
- [5] Liao C-D, Tsai J-C. The evolution of MEMS displays. *IEEE Transactions on Industrial Electronics* 2009;56(4):1057–65.
- [6] Jang B, Hassibi A. Biosensor systems in standard CMOS processes: fact or fiction? *IEEE Transactions on Industrial Electronics* 2009;56(4):979–85.
- [7] Li L, Uttamchandani D. Flip-chip distributed MEMS transmission lines (DMTLs) for biosensing applications. *IEEE Transactions on Industrial Electronics* 2009;56(4):986–90.
- [8] Lin Y-T, Lin Y-S, Chen C-H, Chen HC, Yang Y-C, Lu S-S. A 0.5 V biomedical system-on-a-chip for intra-body communication system. *IEEE Transactions on Industrial Electronics* 2011;58(2):690–9.
- [9] Kuo S-K, Chen S-L, Lin C-T. Design and development of RFID label for steel coil. *IEEE Transactions on Industrial Electronics* 2010;57(6):2180–6.
- [10] Alahmad MA, Hess HL. Evaluation and analysis of a new solid-state rechargeable microscale lithium battery. *IEEE Transactions on Industrial Electronics* 2008;55(9):3391–401.
- [11] Enriquez DAC, Cruz AR, Giraldo MTMR. Hybrid FBG-LPG sensor for surrounding refractive index and temperature simultaneous discrimination. *Optics & Laser Technology* 2012;44(4):981–6.
- [12] Ospina J, Canuto E, Molano Jimenez A, Acuña-Bravo W. Multilayer control of an optical reference cavity for space applications. *IEEE Transactions on Industrial Electronics* 2010;57(7):2507–18.
- [13] Grossman BG, Boonsopa S, Sokol M. Lead-insensitive fiber optic pH sensor and performance under bending. *Optics & Laser Technology* 2005;37(3):199–209.
- [14] Bifano T. MEMS deformable mirrors. *Nature Photonics* 2011;5:21–3.
- [15] Kong S-H, Wijngaards DDL, Wolfenbittel RF. Infrared micro-spectrometer based on a diffraction grating. *Sensors and Actuators A: Elsevier Science* 2001;92:88–95.
- [16] Sakudoa A, Suganumaa Y, Kobayashita T, Onoderac T, Ikuta K. Near-infrared spectroscopy: promising diagnostic tool for viral infections. *Biochemical and Biophysical Research Communications: Elsevier Science* 2006;341:279–84.
- [17] Huang H, Yu H, Xu H, Ying Y. Near infrared spectroscopy for on-line monitoring of quality in foods and beverages: a review. *Journal of Food Engineering: Elsevier Science* 2008;87:303–13.
- [18] Moffat AC, Assi S, Watt RA. Identifying counterfeit medicines using near infrared spectroscopy. *Journal of Near Infrared Spectroscopy* 2010;18:1–15.
- [19] Reeves JB, McCarty GW, Reeves VB. Mid-infrared diffuse reflectance spectroscopy for the quantitative analysis of agricultural soils. *Journal of Agricultural and Food Chemistry* 2001;49(2):766–72.
- [20] Safar M, Bertrand D, Robert P, Devalued MF, Genot C. Characterization of edible oils, butters and margarines by Fourier transform infrared spectroscopy with attenuated total reflectance. *Journal of American Oil Chemists Society* 1994;71(4):371–7.
- [21] Bartick EG. Applications of Vibrational Spectroscopy in Criminal Forensic Analysis. *Handbook of Vibrational Spectroscopy*; 2006.

- [22] Fernandes AV, Cardoso VF, Rocha JG, Minas G. Smart-optical detector CMOS array for biochemical parameters analysis in physiological fluids. *IEEE Transactions on Industrial Electronics* 2008;55(9):3192–200.
- [23] de Hoog J, Osán J, Szalóki I, Eyckmans K, Worobiec A, Ro C-U, Van Grieken R. Thin-windows electron probe X-ray micro-analysis of individual atmospheric particles above the North Sea. *Atmospheric Environment* 2005;39:3231–42.
- [24] de Graaf G, der Vliet W, Wolffenbuttel RF. Design and fabrication steps for a MEMS-based infrared spectrometer using evanescent wave sensing. *Sensors and Actuators A: Elsevier Science* 2008;142:211–6.
- [25] Wolffenbuttel RF. State-of-the-art in integrated optical microspectrometers. *IEEE Transactions on Instrumentation and Measurement* 2004;53(1):197–201.
- [26] Wolffenbuttel RF. MEMS-based optical mini and microspectrometers for the visible and infrared spectral range. *Journal of Micromechanics and Microengineering: Institute of Physics (IOP)* 2005;15:S145–52.
- [27] Emadi A, Wu H, Grabarnik S, de Graaf G, Hedsten K, Enoksson P, Correia JH, Wolffenbuttel RF. Fabrication and characterization of IC-compatible linear variable optical filters with application in a micro-spectrometer. *Journal Sensors and Actuators A: Elsevier Science* 2010;162:400–5.
- [28] Sailaja S, Arora V, Kumbhare SR, Joshi RA, Naik PA, Gupta PD. Transmission grating spectrograph with on-line recording of XUV soft X-ray spectra from laser produced plasmas. *Optics & Laser Technology* 2006;38(1):46–50.
- [29] Liu J, Gao H, Zhou J, Liu D. The design of a polarizing beam splitter made from a dielectric rectangular-groove grating. *Optics & Laser Technology* 2009;41(5):622–626.
- [30] Kloos C. Design of a Michelson interferometer for the measurement of electrostrictive strains. *Optics & Laser Technology* 1996;28(6):481–4.
- [31] Srivastava A, Gupta MM, Medhekar S. Signal amplification based on the local nonlinear Mach-Zehnder interferometer. *Optics & Laser Technology* 2012;44(2):492–496.
- [32] Papadopoulos G, Zoiros KE. On the design of semiconductor optical amplifier-assisted Sagnac interferometer with full data dual output switching capability. *Optics & Laser Technology* 2011;43(3):697–710.
- [33] Wu Z, X G. Transmission of a gaussian beam after incidenting nonnormally on a Fabry-Perot etalon: a nonresonant case. *Optics & Laser Technology* 2003;35(2):123–6.
- [34] Kong S-H, Wolffenbuttel RF. Spectral performance of a micromachined infrared spectrum analyzer in silicon. *IEEE Transactions on Instrumentation and Measurement* 2005;54(1):264–7.
- [35] Grabarnik S, Emadi A, Wu H, de Graaf G, Vdovin G, Wolffenbuttel RF. Fabrication of an imaging diffraction grating for use in a MEMS-based optical microspectrograph. *Journal of Micromechanics and Microengineering* 2008;18(064006):1–6.
- [36] Chien-I Lin Thomas K, Gaylord, loss measurement of plasmonic modes in planar metal-insulator-metal waveguides by an attenuated total reflection method. *Optics Letters* 2010;35(22):3814–6.
- [37] Hass G. Filmed surfaces for reflecting optics. *Journal of Optical Society of America* 1955;45(11):945–53.
- [38] Bartek M, Correia J, Wolffenbuttel RF. Silver-based reflective coatings for micromachined optical filters. *Journal of Micromechanics and Microengineering: Institute of Physics (IOP)* 1999;9:162–5.
- [39] Correia JH, de Graaf G, Bartek M, Wolffenbuttel RF. A CMOS optical microspectrometer with light-to-frequency converter, bus interface and stray-light compensation. *IEEE Transactions Instrumentation & Measurement* 2001;50(6):1530–1537.
- [40] Emadi A, Wu H, Grabarnik S, de Graaf G, Hedsten K, Enoksson P, Correia JH, Wolffenbuttel RF. Fabrication and characterization of IC-compatible linear variable optical filters with application in a micro-spectrometer. *Journal Sensors and Actuators A* 2010;162:400–5.
- [41] Chang, C-P, Huang, R-S, A 16-channel array-type microspectrometer using integrated Fabry-Perot etalons and lateral PIN photodetectors, in *Proc. of IEEE Sensors 2003 (Second IEEE International Conference On Sensors)*, pp.675–678, 2003.
- [42] Rossberg D. Optical properties of the integrated infrared sensor. *Journal Sensors and Actuators A: Elsevier Science* 1996;54:793–7.
- [43] Ribeiro E, Malczyk A, Carvalho S, Rebouta L, Fernandes J, Alves E, Miranda AS. Effects of ion bombardment on properties of d.c. sputtered superhard (Ti, Si, Al)N nanocomposite coatings. *Surface Coating Technology* 2002;515:151–2.
- [44] Sui K-R, Shi Y-W, Tang X-L, Zhu X-S, Iwai K, Miyagi M. Optical properties of Ag/Ag infrared hollow fiber in the visible wavelength region. *Optics Letters* 2008;33:318–20.
- [45] Morichetti F, Canciamilla A, Melloni A. Statistics of backscattering in optical waveguides. *Optics Letters* 2010;35:1777–9.